




## Article

# UV-Light Mediated Biosynthesis of Silver Nanowires; Characterization, Dye Degradation Potential and Kinetic Studies

Faisal Ali <sup>1</sup>, Zahid Ali <sup>1,2</sup>, Umer Younas <sup>1</sup>, Awais Ahmad <sup>3,\*</sup> , Ghulam Mooin-ud-din <sup>1</sup>, Muhammad Pervaiz <sup>4</sup>, Rafael Luque <sup>3,\*</sup> , Ikram Ahmad <sup>5</sup>, Adnan Ashraf <sup>1</sup>, Munirah D. Albaqami <sup>6</sup>, Aboud Ahmed Awadh Bahajjaj <sup>6</sup>  and Muhammad Waqas Ishaq <sup>7,\*</sup>

- <sup>1</sup> Department of Chemistry, The University of Lahore, Lahore 54590, Pakistan; faisal.ali@chem.uol.edu.pk (F.A.); zahid.ali@chem.uol.edu.pk (Z.A.); umer.younas@chem.uol.edu.pk (U.Y.); mooinakram786@gmail.com (G.M.-u.-d.); adnan.ashraf@chem.uol.edu.pk (A.A.)
- <sup>2</sup> State Key Laboratory of High-Performance Carbon Fiber and Functional Polymers, Ministry of Education, Beijing University of Chemical Technology, Beijing 100000, China
- <sup>3</sup> Departamento de Química Organica, Universidad de Cordoba, Edificio Marie Curie (C-3), Ctra Nnal IV-A, Km 396, E14014 Cordoba, Spain
- <sup>4</sup> Department of Chemistry, Government College University, Lahore 54000, Pakistan; mpbhatti786@gmail.com
- <sup>5</sup> Department of Chemistry, University of Sahiwal, Sahiwal 57000, Pakistan; drikramahmad@uosahiwal.edu.pk
- <sup>6</sup> Department of Chemistry, College of Science, King Saud University, Riyadh 11451, Saudi Arabia; muneerad@ksu.edu.sa (M.D.A.); aawadh@ksu.edu.sa (A.A.A.B.)
- <sup>7</sup> Department of Chemical Physics, University of Science and Technology of China, Hefei 230000, China
- \* Correspondence: awaisahmed@gcuf.edu.pk (A.A.); q62alsor@uco.es (R.L.); mwaqasmayo@hotmail.com (M.W.I.)



**Citation:** Ali, F.; Ali, Z.; Younas, U.; Ahmad, A.; Mooin-ud-din, G.; Pervaiz, M.; Luque, R.; Ahmad, I.; Ashraf, A.; Albaqami, M.D.; et al. UV-Light Mediated Biosynthesis of Silver Nanowires; Characterization, Dye Degradation Potential and Kinetic Studies. *Sustainability* **2021**, *13*, 13220. <https://doi.org/10.3390/su132313220>

Academic Editor: Rajesh Kumar Jyothi

Received: 18 October 2021  
Accepted: 23 November 2021  
Published: 29 November 2021

**Publisher's Note:** MDPI stays neutral with regard to jurisdictional claims in published maps and institutional affiliations.



**Copyright:** © 2021 by the authors. Licensee MDPI, Basel, Switzerland. This article is an open access article distributed under the terms and conditions of the Creative Commons Attribution (CC BY) license (<https://creativecommons.org/licenses/by/4.0/>).

**Abstract:** Herrin, a simple and eco-friendly method for the synthesis of silver nanowires (Ag-NWs) has been reported. Silver nanowires were synthesized using *Psidium guajava* seed extract that acted as a reducing agent as well as a stabilizing agent for silver nitrate solution. Synthesis was carried out at 50 °C temperature under continuous UV-irradiation. Silver nanowires were initially characterized by a UV-visible and FTIR spectrophotometer. In addition, morphology and particle size of synthesized Ag-NWs were determined using Field Emission Scanning Electron Microscopy and X-ray diffraction (XRD) techniques. Nanowires were found to have 12.8 μm length and 200–500 nm diameter and cubic phase morphology. Furthermore, the catalytic potential of Ag-NWs for the degradation of methyl orange dye (MO) was determined. The selected dye was degraded successfully that confirmed the catalytic potential of Ag-NWs. The authors concluded that Ag-NWs can be synthesized using plant extract having excellent morphological features as well as impressive catalytic potential.

**Keywords:** catalytic degradation; methyl orange dye; silver nanowires; degradation kinetics

## 1. Introduction

Synthetic organic dyes have been reported to cause countless serious threats to the ecosystem and human health as a huge amount of these chemicals is being used on daily basis. The tremendous growth of textile industries has increased the use of dyes as well as pigments [1–3]. The effluents from such industries are usually discharged into the environment without treatment, which alters the composition of surface and ground water and risks the health of living beings. With the passage of time, dyes in an aqueous medium undergo chemical degradation followed by transformation to toxic chemical entities [4]. The degradation products of dyes indirectly or directly enter the food web and originate unadorned toxic impacts on living beings.

A number of techniques have been reported for the removal of synthetic dyes from effluents such as catalytic reduction [5], adsorption [6], membrane matrices [7], bio-remediation [8] and advanced oxidation routes include photolysis and photocatalysis [9]. Among these,

photocatalytic degradation of dyes using metal nano-catalyst is one of the prime methods that has been focused on these days due to its efficiency and cost-effectiveness [10,11]. The reduction of such dyes by metal nanoparticles produces biodegradable products [10]. Metal-based nano-catalysts for such reduction are mainly derived from noble metals, like Ag and Au [12,13] due to their extraordinary stability and high specific area. Several routes for the synthesis of metal nanoparticles including co-precipitation [14–16], hydrothermal synthesis [17], sol-gel method [18], inert gas condensation [19], laser ablation [20], sputtering [21], template synthesis [22], electron irradiation with heating [23] and biological synthesis [24] have been developed. However, biological synthesis is the hot choice with advantages over physical and chemical methods as it is quick, eco-friendly, highly stable and cost-effective [25].

Catalytic degradation mainly depends upon the morphology [26] and surface area of the nanostructures [27], that is, nanoparticles [28], nano-rods [29], nano-spheres [30], nanotubes [31] and nanowires [32]. Among them, nanowires have grabbed the prime focus of material scientists due to their excellent features like surface area, micro-porous structural features, the highest contact area with adsorbate surfaces [33]. Lin Bao et al. have reported the synthesizes of nanowires via green approach by using poly-vinyl acetate (PVA) polymer back-bone as a stabilizing agent due to the lower stability of Ag-nanowires (Ag-NWs) [34]. Many serious attempts have been made to enhance the stability of Ag-NW by using stabilizers like polymer matrices (PVA, PPy EG and glucose) [35], ITO glass electrode base [36] and electrostatic charge stabilizers [37]. The synthesis of Ag-NW via a facile, green and eco-friendly routes without any external stabilizers and pro-longed shelf-life is still a great challenge for scientists [38].

In this manuscript, we are reporting a facile and green approach to synthesize the Ag-Nanowires (Ag-NW) using *Psidium guajava* seed extract. In order to stabilize nanowires no external stabilizers, like ITO-glass electrodes, electrostatic charge, have been used. Characterization of nanowires was carried out by employing spectroscopic techniques such as VU-visible, FTIR, SEM and XRD. The catalytic potential of Ag-NWs was evaluated by studying their ability to remove methyl orange (MO) from an aqueous medium.

## 2. Materials and Methods

### 2.1. Materials

Silver nitrate (99.9%) was acquired from Merck, Germany, sodium hydroxide (NaOH) (80%) and sodium borohydride ( $\text{NaBH}_4$ ) (97%) was purchased from Sigma Aldrich, Dorset, UK. The methyl orange dye (87%) was purchased from Pakistan Ltd. (Fisher, Lahore). All chemicals were used without further purification. Double deionized water was used throughout the analysis.

### 2.2. Preparation of *Psidium Guajava* Seeds Extract

*Psidium guajava* seeds were collected washed and dried in an oven around 50 °C till 48 h. *Psidium guajava* seeds were powdered using a grinder and powder of 0.40 micron was collected using specific sieves. *Psidium guajava* seeds (0.1 g) were taken in a flask and 100 mL distilled water was added followed by constant stirring at 40 °C temperature for 50 min [39]. After filtration, the plant extract was collected and concentrated using a rotary evaporator [40].

### 2.3. Synthesis of Silver Nanowires

In order to prepare Ag-NWs, *Psidium guajava* seeds extract (5 mL) was added into the aqueous solution of  $\text{AgNO}_3$  (1 Mm/10 mL) under standard conditions. The mixture was constantly stirred at 50 °C with continuous irradiation of UV-light of 265 nm for four hours. The color change from milky white to yellow and finally orange indicated the formation of the silver nanowires [41]. Ag-nanowires were collected after filtration followed by oven drying at 50 °C for 30 min (Figure 1A,B).

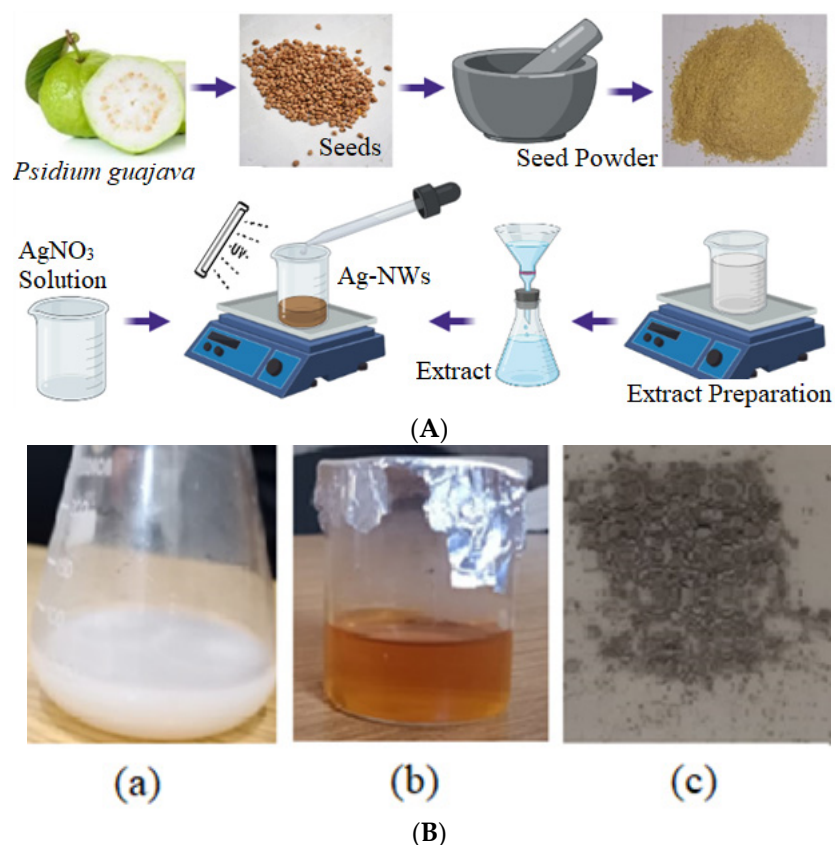


**Figure 1.** (A). Step-wise representation for the formation of Silver-Nanowires (Ag-NWs) by using *Psidium guajava* seeds extract under UV-irradiation. (B). Extract +  $\text{AgNO}_3$  solution (a), Orange colored Ag-NWs (b), Ag-NWs powder (c).

#### 2.4. Characterization of Ag Nanowire

The fabrication of Ag-NWs was preliminarily established by recording the absorbance in UV/Vis spectra at a range of 300–800 nm. The change in Surface Plasmon Resonance (SPR) of nanoparticles in the dispersion was recorded using UV/Vis spectrophotometer. The XRD patterns of Ag-nanowires were collected on Bruker AXS-D8 Advanced X-ray diffractometer with  $\text{Cu K}\alpha$  radiations of  $\lambda = 1.5406 \text{ \AA}$  and scanning angle  $2\theta$  over the range of  $10\text{--}80^\circ$ . Crystallite size was calculated by using Scherer Equation  $CS = K\lambda/\beta \cos \theta$ , where CS is the crystallite size, constant  $K = 0.94$ ,  $\beta$  is the full width at half maximum (FWHM), ( $\beta = \text{FWHM} \times \pi/180$ ),  $\lambda = 1.5406 \times 10^{-10}$ . and  $\cos \theta = \text{Bragg's angle}$ . Fourier Transformation Infrared Spectroscopy (FTIR) was used to characterize the nanoparticles using the powder sample by ATR in the range of  $400\text{--}4000 \text{ cm}^{-1}$ . Scanning electron microscopy (SEM) images were recorded using FEI-NOVA-450 Nano-SEM (FE-SEM) by the USA (Hillsboro, ORE, USA). The functional group determination was carried out by utilizing Alpha-II FTIR-ATR by BRUKERS Internationals (Urbandale, IA, USA).

#### 2.5. Catalytic Potential of Ag-NWs

In order to evaluate the catalytic potential of Ag-NWs, degradation of methyl orange (MO) dye was conducted in the presence of Ag-NWs. Sodium borohydride (0.6 mL of 17.6 mM) along with Ag-NWs as catalyst (0.4 mL of 0.64 to 3.84 mg/mL) was used for dye degradation (1.6 mL of 0.062 to 0.102 mM). Reaction mixtures with and without Ag-NWs were monitored using UV/Vis spectra from 300–800 nm every 2 min.

### 3. Results and Discussion

#### 3.1. UV-Visible Analysis of Ag-NWs

UV-visible spectroscopy is a convenient and preliminary method for the characterization of nanomaterials [42]. The Ag-nanowires bands show a strong absorption band and produce certain colors due to the surface plasma resonance appearing at 435.0 nm with a progressive increase in absorbance for 30 min (Figure 2) [43]. The characteristic absorption peak for Ag-nanowires synthesized by any method is reported from 300–440 nm ranges which is due to the oscillation of electrons in the conduction band [44,45]. Moreover, the trapped electron can also be involved in intra-center transitions between  $\text{Ag}^0/\text{Ag}^+$ , due to which the absorption band could appear in the 440–550 nm range [46]. It is clear from spectra that there is no peak in *Psidium guajava* seed extract solution which illustrates the absence of Ag-NWs. But after mixing  $\text{AgNO}_3$  solution with Guajava extract, a change in color to yellowish-brown represented the reduction of silver ion and a peak appeared at around 435.0 nm due to surface plasma resonance that confirmed the synthesis of nanowires [47].

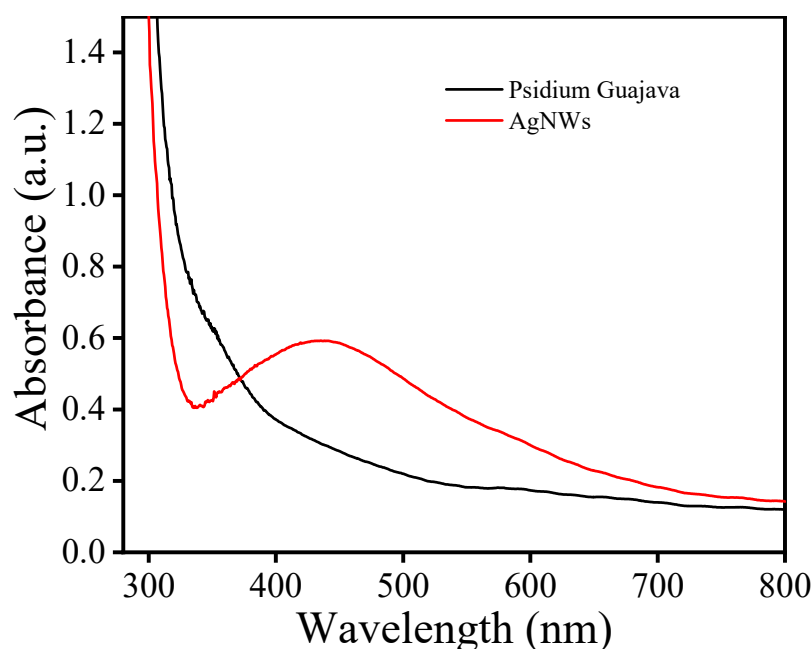
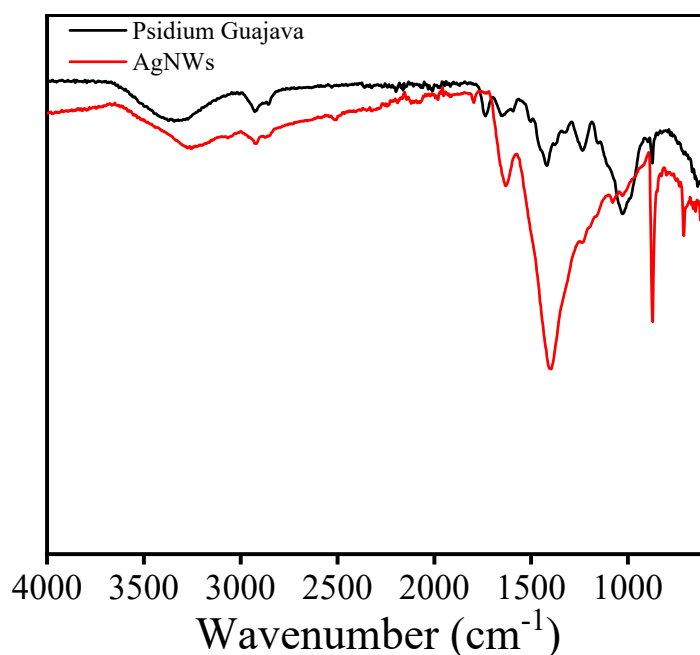


Figure 2. UV/Vis spectra of *P. guajava* extract and Ag-NWs.

The increase in absorption from 300 nm (Figure 2) corresponded to the development of different sizes of silver nanowires.

#### 3.2. FTIR Studies of Ag NWs

FTIR analysis of *P. guajava* extract and Ag-NWs was conducted to find out the functional groups accountable for the reduction and capping of silver ions (Figure 3). The existence of peaks at  $3400\text{--}3300\text{ cm}^{-1}$  and  $1600\text{ cm}^{-1}$  may perhaps be due to  $\text{--OH}$  stretching of the alcohol and carboxylic acids, respectively [48,49]. The peak  $3400\text{--}3300\text{ cm}^{-1}$  was shifted towards a shorter wavelength after reacting with silver, maybe due to the interaction of Ag with the carboxylic acid  $\text{--OH}$  group present in the extract [50,51]. The peaks around  $2197\text{ cm}^{-1}$  and  $1619\text{ cm}^{-1}$  affirm the presence of  $\alpha$ ,  $\beta$ -substituted unsaturated carbonyl group-containing entities. Two peaks observed at  $2161\text{ cm}^{-1}$  and  $2009\text{ cm}^{-1}$  confirm the iso-cyanate and thio-cyanate functionalities, respectively [52,53]. The peaks at  $1735\text{ cm}^{-1}$  and  $1647\text{ cm}^{-1}$  confirm the presence of ortho-substituted six-membered lactone. The  $\text{--OH}$  bending of  $\alpha$ ,  $\beta$ -unsaturated carboxylic was recorded at  $1430\text{--}1400\text{ cm}^{-1}$  and it becomes stronger in the case of Ag-NWs [53–55]. The hydrogen bonding between  $\text{--OH}$  group of nanostructures and  $\alpha$ ,  $\beta$ -unsaturated carboxylic acts to reduce silver nitrate to silver ions and also works as a capping agent and stabilizes the Ag-NWs [49] (Table 1).



**Figure 3.** FTIR analysis of *Psidium guajava* extract and Ag-NWs.

**Table 1.** Functional group identifications with adsorption peaks of FTIR spectra.

Sr. No.	Absorption Peaks	Functional Groups	References
1	3400–3300 $\text{cm}^{-1}$ and 1600 $\text{cm}^{-1}$	—OH stretching of the alcohol and carboxylic acids	[49]
2	2197 $\text{cm}^{-1}$ and 1619 $\text{cm}^{-1}$	$\alpha$ , $\beta$ -substituted unsaturated carbonyl	
3	2161 $\text{cm}^{-1}$	iso-cyanate	
4	2009 $\text{cm}^{-1}$	thio-cyanate	
5	1735 $\text{cm}^{-1}$ and 1647 $\text{cm}^{-1}$	ortho-substituted six-membered lactone	
6	1430–1400 $\text{cm}^{-1}$	—OH bending of $\alpha$ , $\beta$ -unsaturated carboxylic	
7	1435 $\text{cm}^{-1}$	-C=C linkages	

### 3.3. SEM Analysis of Ag-NWs

The morphology and surface properties of the product were determined by field emission scanning electron microscopy (FE-SEM) (Figure 4a–d). It is evident that the product has a wire-like morphology mainly formed and stabilized due to the action of unsaturated linear ketones. The well-separated wires have  $\sim 12.8 \mu\text{m}$  length and  $\sim 200\text{--}500 \text{ nm}$  diameter. This unique morphology results in an excellent surface area expansion, resulting in brilliant catalytic removal of the organic dyes. The performance of a catalyst is chiefly dependent on the surface area, stability, surface charge and shape of the molecules of a catalyst. Amongst them, surface area and shape have been shown to have a more powerful role in the adsorption and reduction of the adsorbed entities in photocatalysis phenomena as mentioned in previous works [56].

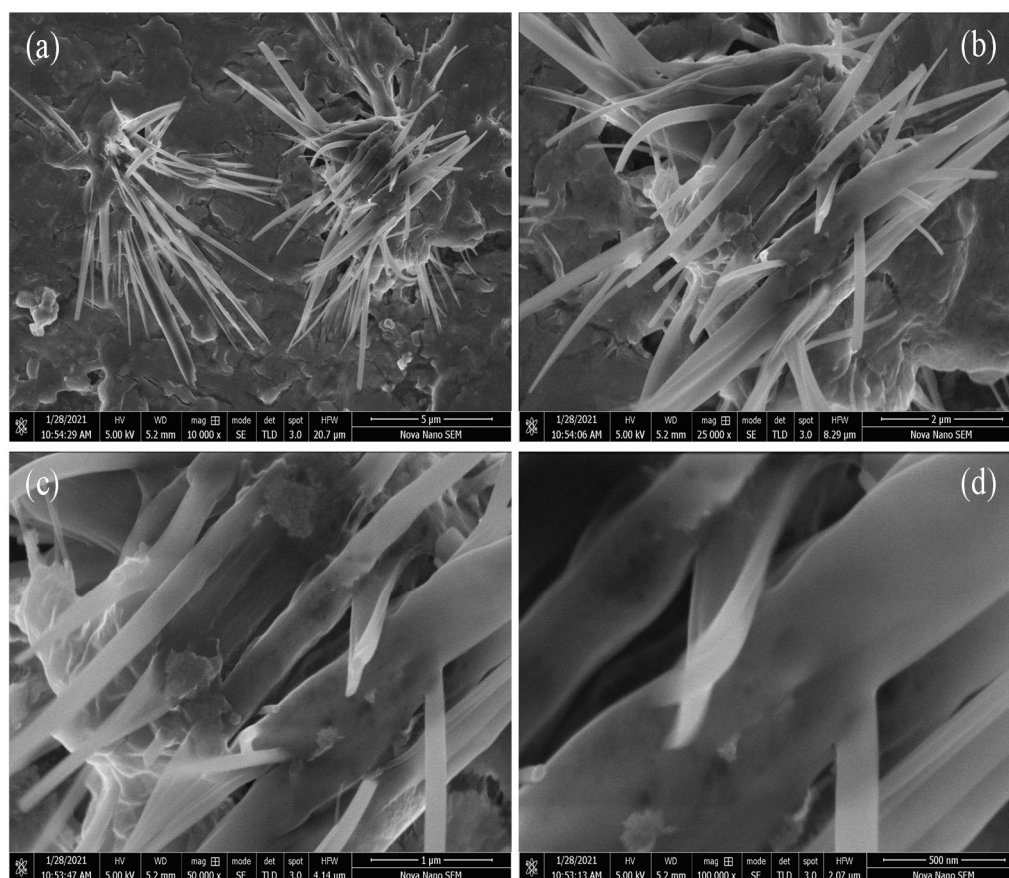


**Figure 4.** FE-SEM images of Ag-NWs stabilized *Psidium guajava* seeds at different resolution (a) 5  $\mu\text{m}$  (b) 2  $\mu\text{m}$  (c) 1  $\mu\text{m}$  (d) 500 nm.

### 3.4. XRD Analysis of Ag-NWs

Silver nanowires were also characterized using the X-ray diffraction method to elucidate the structure (Figure 5). The fingerprint pattern has four typical diffraction features corresponding to (111), (200), (020), (220) and (131) planes, and all the four peaks might be indexed to the phase-centered cubic structure of silver (JCPDS-04-0783) [57,58]. The final product owes 100% purity as there was no peak detected for reflection, which mainly corresponds to nitrate ions of precursor solution and other impurities. The peak intensity profile was individual of the face-centered cuboidal structure of Ag-nanowires. The crystallite size is not entirely clear in FESEM due to the large nanowire diameter [59]. However, the particle size is calculated by the Debye–Sherrer Equation.

$$D_{avg} (nm) = \frac{K\lambda}{\beta \cos\theta} \quad (1)$$

where  $D_{avg}$  is the average crystallite size, constant  $K$  is the shape factor (0.9),  $\lambda$  is the wavelength (0.154 nm),  $\beta$  corresponds to the peak width at half maximum intensity while  $\theta$  is the peak position. The  $D_{avg}$  Ag-NWs is 24.83 nm, which is quite close to the reported one (30–35 nm) [59,60].

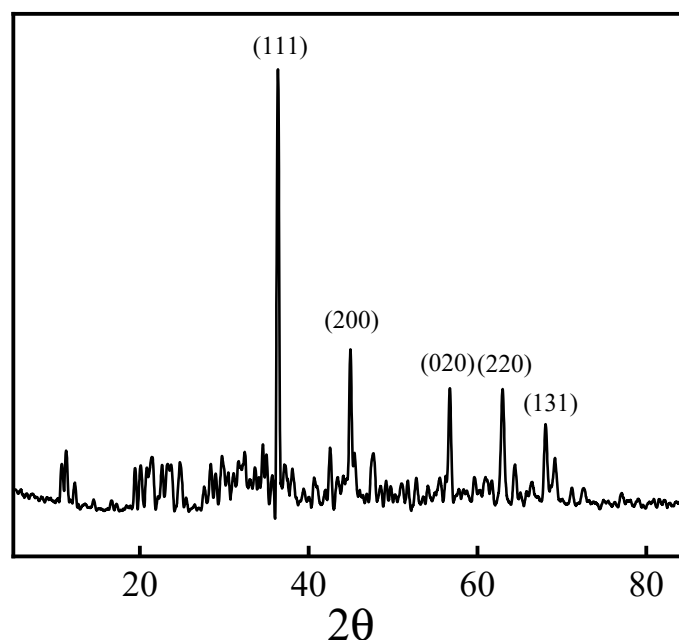


**Figure 5.** XRD pattern of Ag-NWs.

### 3.5. Catalytic Potential of Ag-NWs

Methyl Orange (MO) is extensively used as a textile dye (azo-dye) for the dyeing of textile fabrics [61]. The reduction of MO was achieved by using freshly prepared Ag-NWs with excessive  $\text{NaBH}_4$ . The rate of reduction of methyl orange without catalyst in the presence of  $\text{NaBH}_4$  is very slow (Figure 6a). This poor performance is due to the presence of a high energy barrier of mutually repulsive interactions between the borohydride anion and methyl orange ion, which should be overcome only by a catalyst [62]. Moreover, in the presence of a catalyst only no reduction occurs due to the same interactions as mentioned above (Figure 6b). However, in the presence of a catalyst and  $\text{NaBH}_4$ , reduction of azo-dye takes place (Model reaction). Initially,  $\text{NaBH}_4$  and catalyst will adsorb on the surface of the dye and then a reduction reaction will proceed at a faster rate. The characteristic peak of MO solution was recorded  $\sim 458$  nm and catalytic reduction was observed by a sharp decline in intensity merely in 25 min (Figure 6c).

### 3.6. Kinetic Studies of Dye Degradation Reactions

#### 3.6.1. Effect of Catalyst Dosage

The effect of concentration of catalyst-dosage was determined by changing the amount of Ag-NWs from 0.60–3.84 mg/mL added to the reaction mixture. It is evident from Figure 7a, that from 0 to 5 min, the reaction started with a very slow speed as there are molecules moving towards the surface of Ag-NWs and speed up from 6 to 20 min due to their interaction at the surface of the catalyst, then ultimately reaches to completion after 20–25 min. The inset graph shows the negative slopes used for the determination of  $k_{\text{obs}}$  [63].

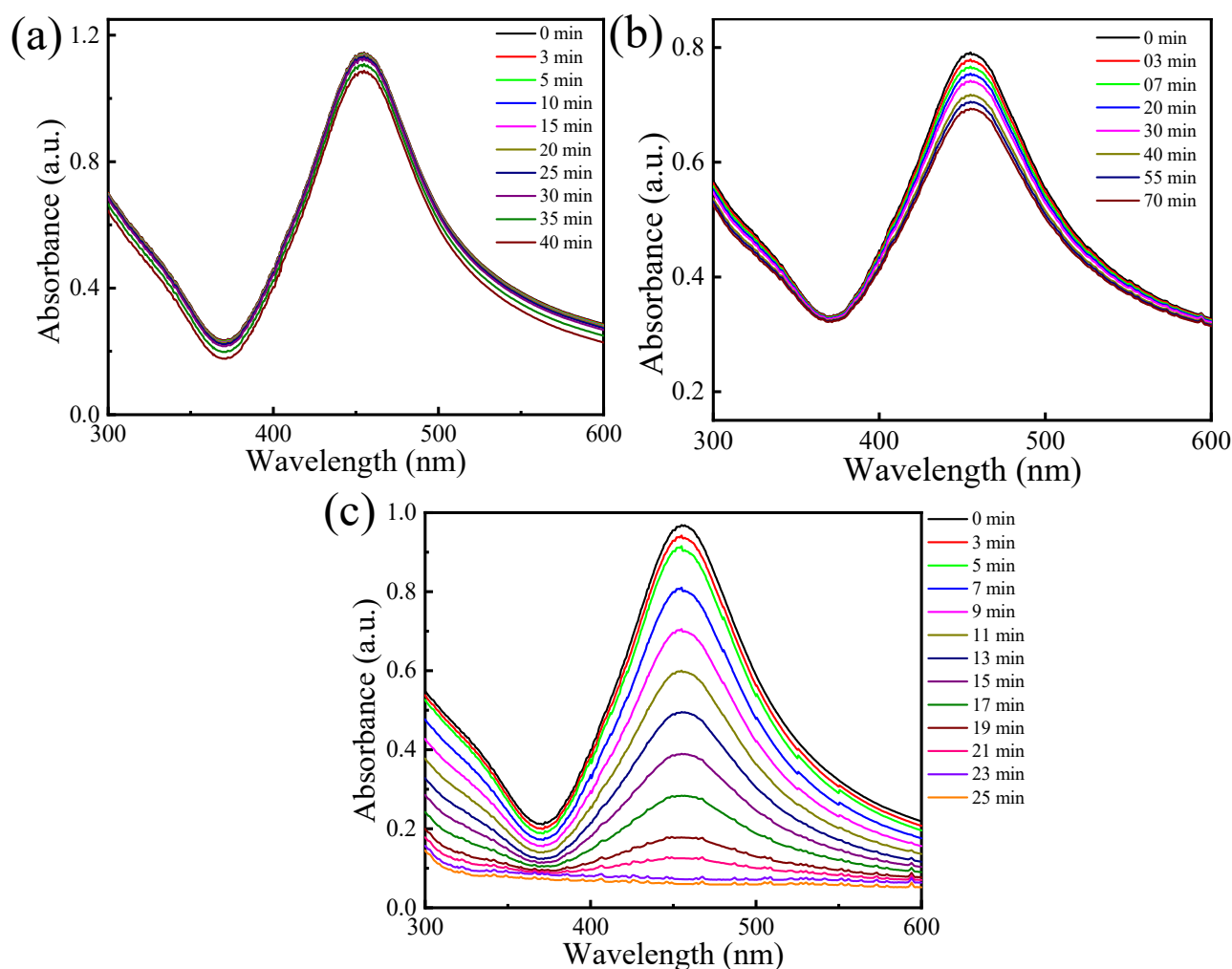


**Figure 6.** In the absence of catalyst (a), in the absence of  $\text{NaBH}_4$  (b) Degradation reaction having  $\text{NaBH}_4 = [17.6 \text{ mM}]$ ,  $\text{MO} = [0.082 \text{ mM}]$ ,  $\text{Ag-NW (catalyst)} = [1.84 \text{ mg/mL}]$  (c).

It is evident from Figure 7b, the rate of reaction increases fast from 0.60–1.28 mg/mL because the degradation takes place exponentially at the start of the reaction due to the presence of active sites. Later on, the reaction rate becomes slow from 2.56–3.84 mg/mL due to occupied active sites [64]. The most effective degradation out of all the adsorbents' concentrations was monitored at 1.28 mg/mL with the help of  $k_{\text{obs}}$  graph plotted between  $k_{\text{obs}}$  vs concentration of Ag-NWs while keeping the  $\text{NaBH}_4$  concentration (17.6 mM) and MO-dye (0.082 mM) constant. The half-life (min) of the observed rate constant ( $\text{min}^{-1}$ ) calculated for these pseudo-first-order reactions is mentioned in Table 1.



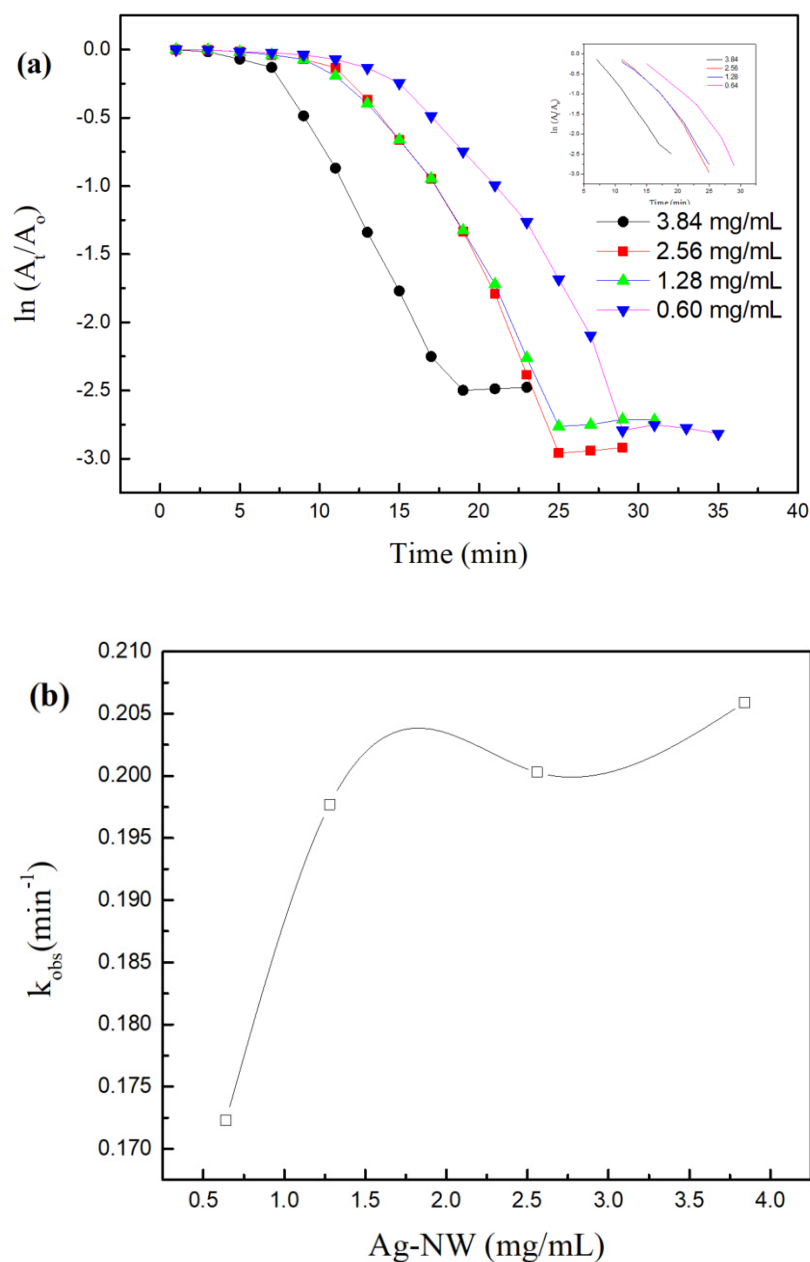


**Figure 7.** Effect of Ag-NWs-Catalyst dosage on extent of dye degradation reaction and inset shows degradation reaction kinetics (a) and  $k_{obs}$  determination (b).

### 3.6.2. Effect of MO Dye

MO dye's concentrations were taken, ranging from 0.072 to 0.102 mM with 0.010 mM difference. Figure 8a shows the induction, reaction and completion times of the catalytic reaction between MO-dye and  $\text{NaBH}_4$  on the surface of Ag-NWs. As the concentration of the MO-dye increases, while keeping the concentrations of Ag-NWs and  $\text{NaBH}_4$  constant, the time of degradation increases [65]. The reason behind this factor is the constant concentration of Ag-NWs, which illustrates the limitation of surface-active sites for incoming reactants [66]. The figure inset (6) shows the negative slopes for finding the apparent rate constant for Pseudo first-order reaction following the Langmuir–Hinshelwood mechanism (LHM) [67,68].

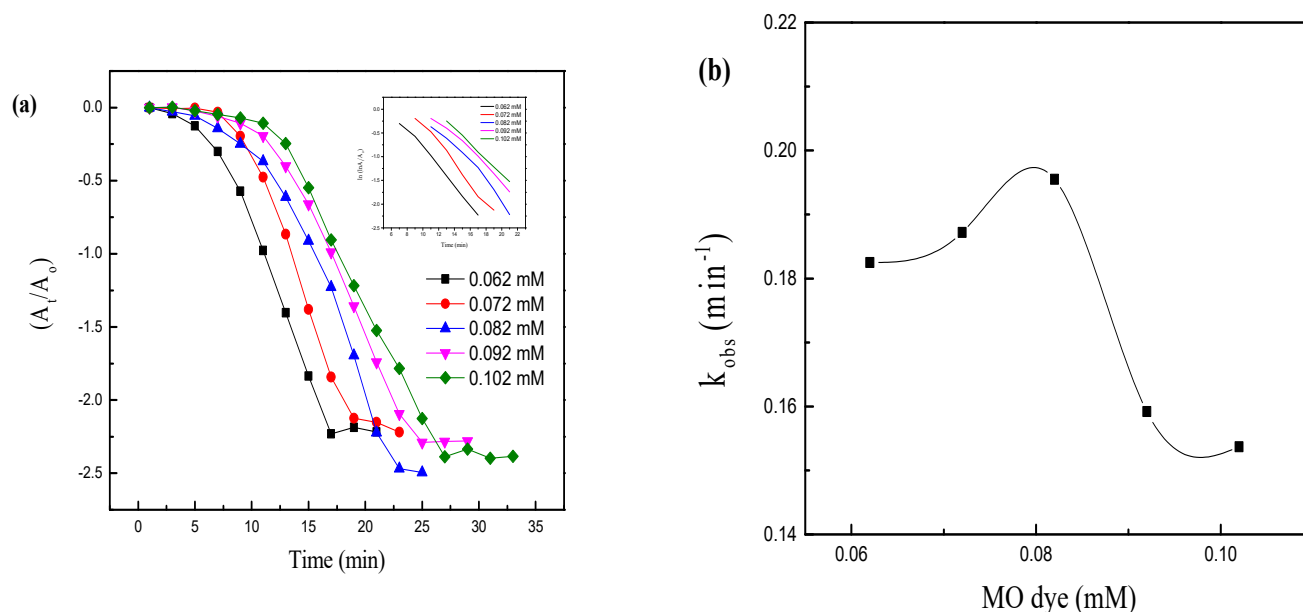


**Figure 8.** Effect of MO dye concentration on degradation reaction and inset shows degradation reaction kinetics (a) and observed-rate constant determination (b).

Figure 8b, illustrates the graph between  $k_{obs}$  on ordinate and concentration of MO-dye on abscissa while keeping catalyst dosage (1.28 mg/mL) and  $\text{NaBH}_4$  (17.6 mM) constant.

This graph explains that initially, the  $k_{obs}$  value remains constant while, at 0.082 mM its concentration increases to the maximum  $k_{obs}$  value. This is due to the maximum adsorption of the incoming MO-dye molecules on the surface catalytically enhanced by Ag-NWs. This point is fruitful in the optimization of reaction. After this concentration, the decrease in  $k_{obs}$  value is due to the excessive amount of MO-dye molecules on the surface of limited Ag-NWs. Here, the double-layer adsorption occurs on the surface of Ag-NWs, which restricts the effective adsorption. Half-life (min) and  $k_{obs}$  values were calculated and incorporated in Table 2.

**Table 2.** Values of Observed rate constant ( $k_{obs}$ ) for MO degradation using different catalysts dose, concentrations of  $\text{NaBH}_4$  and MO dye at 27 °C.

Factor	Ag-NWs (mg/mL)	$\text{NaBH}_4$ (mM)	MO Dye (mM)	$k_{obs}$ ( $\text{min}^{-1}$ )	Half-Life Period ( $t_{1/2}$ ) ( $\text{min}^{-1}$ )	$R^2$
Ag-NWs	0.60	17.6	0.082	0.1723	2.1032	0.98
	1.28	17.6	0.082	0.1977	3.5053	0.98
	2.56	17.6	0.082	0.2003	3.4598	0.99
	3.84	17.6	0.082	0.2059	3.3657	0.99
MO dye	0.062	17.6	0.062	0.1825	3.7972	0.97
	0.072	17.6	0.072	0.1872	3.7019	0.98
	0.082	17.6	0.082	0.1955	3.5447	0.99
	0.092	17.6	0.092	0.1592	4.3530	0.98
	0.102	17.6	0.102	0.1537	4.5087	0.97

#### 4. Conclusions

The Ag-NWs were successfully fabricated using  $\text{AgNO}_3$  as a precursor and *Psidium guajava* seed extract under continuous irradiation of UV light. The extract strongly acted as a reducing as well as a stabilizing agent. UV-visible spectra confirm the formation of the Ag-NWs. The average crystallite size of Ag-NWs was 196.4 nm, and the morphology was cubic face having 12.8  $\mu\text{m}$  length and internal diameter of 200–500 nm. Synthesized Ag-NWs was then used for the catalytic degradation MO-dye,  $\text{NaBH}_4$  and Ag-NWs. This

study proposed reaction completion merely in 25 min and kinetic studies of the data confirmed pseudo-first-order reaction. Hence, *Psidium guajava* seed extract can be used for the synthesis of Ag-NWs. The authors recommended that Ag-NWs can be exploited for the degradation of azo-dyes that can be a good tool for the treatment of water from the textile industry.

## 5. Highlights

- UV-light-mediated green synthesis of Ag-NWs using *Psidium guajava* seed extract.
- Dimensions of Ag-NWs were 12–8  $\mu\text{m}$  length and 200–500 nm diameter.
- Morphology of Ag-NWs was confirmed by SEM and XRD.
- Methyl orange dye degradation was achieved using Ag-NWs.
- Kinetics of degradation reaction was studied.

**Author Contributions:** Conceptualization, F.A. and U.Y.; methodology, M.P.; software, A.A. (Adnan Ashraf); validation, I.A., G.M.-u.-d. and M.W.I.; formal analysis, M.D.A.; investigation, A.A.A.B.; resources, I.A.; data curation, I.A.; writing—original draft preparation, A.A. (Awais Ahmad); writing—review and editing, R.L.; visualization, Z.A.; supervision, R.L. All authors have read and agreed to the published version of the manuscript.

**Funding:** This work was funded by the Researchers Supporting Project Number (RSP-2021/267) King Saud University, Riyadh, Saudi Arabia.

**Institutional Review Board Statement:** Not applicable.

**Informed Consent Statement:** Not applicable.

**Data Availability Statement:** Not applicable.

**Conflicts of Interest:** The authors declare no conflict of interest.

## References

1. Mance, G. *Pollution Threat of Heavy Metals in Aquatic Environments*; Springer Science & Business Media: Cham, Switzerland, 2012.
2. Wang, X.; Pei, Y.; Lu, M.; Lu, X.; Du, X. Highly efficient adsorption of heavy metals from wastewaters by graphene oxide-ordered mesoporous silica materials. *J. Mater. Sci.* **2015**, *50*, 2113–2121. [[CrossRef](#)]
3. Ahmad, A.; Jini, D.; Aravind, M.; Parvathiraja, C.; Ali, R.; Kiyani, M.Z.; Alothman, A. A novel study on synthesis of egg shell based activated carbon for degradation of methylene blue via photocatalysis. *Arab. J. Chem.* **2020**, *13*, 8717–8722. [[CrossRef](#)]
4. Chang, Y.-C.; Chen, D.-H. Catalytic reduction of 4-nitrophenol by magnetically recoverable Au nanocatalyst. *J. Hazard. Mater.* **2009**, *165*, 664–669. [[CrossRef](#)]
5. Saleem, M.; Irfan, M.; Tabassum, S.; Albaqami, M.D.; Javed, M.S.; Hussain, S.; Pervaiz, M.; Ahmad, I.; Ahmad, A.; Zuber, M. Experimental and theoretical study of highly porous lignocellulose assisted metal oxide photoelectrodes for dye-sensitized solar cells. *Arab. J. Chem.* **2021**, *14*, 102937. [[CrossRef](#)]
6. Qiu, F.; Tang, R.; Zuo, X.; Shi, X.; Wei, Y.; Zheng, X.; Dai, Y.; Gong, Y.; Wang, L.; Xu, P.; et al. A genome-wide association study identifies six novel risk loci for primary biliary cholangitis. *Nat. Commun.* **2017**, *8*, 14828. [[CrossRef](#)] [[PubMed](#)]
7. Bibi, S.; Ahmad, A.; Anjum, M.A.R.; Haleem, A.; Siddiq, M.; Shah, S.S.; Al Kahtani, A. Photocatalytic degradation of malachite green and methylene blue over reduced graphene oxide (rGO) based metal oxides (rGO-Fe<sub>3</sub>O<sub>4</sub>/TiO<sub>2</sub>) nanocomposite under UV-visible light irradiation. *J. Environ. Chem. Eng.* **2021**, *9*, 105580. [[CrossRef](#)]
8. Kashif, M.; Jaafar, E.; Bhadja, P.; Low, F.W.; Sahari, S.K.; Hussain, S.; Loong, F.K.; Ahmad, A.; AlGarni, T.S.; Shafa, M.; et al. Effect of potassium permanganate on morphological, structural and electro-optical properties of graphene oxide thin films. *Arab. J. Chem.* **2021**, *14*, 102953. [[CrossRef](#)]
9. Liu, C.; Wu, P.; Tran, L.; Zhu, N.; Dang, Z. Organo-montmorillonites for efficient and rapid water remediation: Sequential and simultaneous adsorption of lead and bisphenol A. *Environ. Chem.* **2018**, *15*, 286. [[CrossRef](#)]
10. Hassan, S.S.; Solangi, A.R.; Agheem, M.H.; Junejo, Y.; Kalwar, N.H.; Tagar, Z.A. Ultra-fast catalytic reduction of dyes by ionic liquid recoverable and reusable mafenamic acid derived gold nanoparticles. *J. Hazard. Mater.* **2011**, *190*, 1030–1036. [[CrossRef](#)] [[PubMed](#)]
11. Hu, H.; Xin, J.H.; Hu, H.; Wang, X.; Miao, D.; Liu, Y. Synthesis and stabilization of metal nanocatalysts for reduction reactions—A review. *J. Mater. Chem. A* **2015**, *3*, 11157–11182. [[CrossRef](#)]
12. Wang, P.; Huang, B.; Qin, X.; Zhang, X.; Dai, Y.; Wei, J.; Whangbo, M.H. Ag@AgCl: A highly efficient and stable photocatalyst active under visible light. *Angew. Chem. Int. Ed.* **2008**, *47*, 7931–7933. [[CrossRef](#)] [[PubMed](#)]
13. Yasin, S.; Liu, L.; Yao, J. Biosynthesis of silver nanoparticles by bamboo leaves extract and their antimicrobial activity. *J. Fiber Bioeng. Inform.* **2013**, *6*, 77–84.

14. Kim, Y.I.; Kim, D.; Lee, C.S. Synthesis and characterization of CoFe<sub>2</sub>O<sub>4</sub> magnetic nanoparticles prepared by temperature-controlled coprecipitation method. *Phys. B Condens. Matter* **2003**, *337*, 42–51. [[CrossRef](#)]
15. Khan, M.; Janjua, N.K.; Khan, S.; Qazi, I.; Ali, S.; Saad Algarni, T. Electro-oxidation of ammonia at novel Ag<sub>2</sub>O–PrO<sub>2</sub>/γ-Al<sub>2</sub>O<sub>3</sub> catalysts. *Coatings* **2021**, *11*, 257. [[CrossRef](#)]
16. Khan, S.; Shah, S.S.; Anjum, M.A.; Khan, M.R.; Janjua, N.K. Electro-oxidation of ammonia over copper oxide impregnated γ-Al<sub>2</sub>O<sub>3</sub> nanocatalysts. *Coatings* **2021**, *11*, 313. [[CrossRef](#)]
17. Daou, T.J.; Pourroy, G.; Bégoin-Colin, S.; Grenèche, J.M.; Ulhaq-Bouillet, C.; Legaré, P.; Bernhardt, P.; Leuvrey, A.C.; Rogez, G. Hydrothermal Synthesis of Monodisperse Magnetite Nanoparticles. *Chem. Mater.* **2006**, *18*, 4399–4404. [[CrossRef](#)]
18. Liu, C.; Zou, B.; Rondinone, A.; Zhang, Z.J. Sol–Gel Synthesis of Free-Standing Ferroelectric Lead Zirconate Titanate Nanoparticles. *J. Am. Chem. Soc.* **2001**, *123*, 4344–4345. [[CrossRef](#)] [[PubMed](#)]
19. Pérez-Tijerina, E.; Pinilla, M.G.; Mejía-Rosales, S.; Ortiz-Méndez, U.; Torres, A.; José-Yacamán, M. Highly size-controlled synthesis of Au/Pd nanoparticles by inert-gas condensation. *Faraday Discuss.* **2007**, *138*, 353–362. [[CrossRef](#)]
20. Amendola, V.; Meneghetti, M. Laser ablation synthesis in solution and size manipulation of noble metal nanoparticles. *Phys. Chem. Chem. Phys.* **2009**, *11*, 3805–3821. [[CrossRef](#)] [[PubMed](#)]
21. Rane, A.V.; Kanny, K.; Abitha, V.; Thomas, S. Methods for synthesis of nanoparticles and fabrication of nanocomposites. In *Synthesis of Inorganic Nanomaterials*; Elsevier: Amsterdam, The Netherlands, 2018; pp. 121–139.
22. Sreeram, K.J.; Nidhin, M.; Nair, B.U. Microwave assisted template synthesis of silver nanoparticles. *Bull. Mater. Sci.* **2008**, *31*, 937–942. [[CrossRef](#)]
23. Kotomin, E.; Kuzovkov, V.; Popov, A.I. The kinetics of defect aggregation and metal colloid formation in ionic solids under irradiation. *Radiat. Eff. Defects Solids* **2001**, *155*, 113–125. [[CrossRef](#)]
24. Devi, T.P.; Kulanthaivel, S.; Kamil, D.; Borah, J.L.; Prabhakaran, N.; Srinivasa, N. Biosynthesis of silver nanoparticles from *Trichoderma* species. *Indian J. Exp. Boil.* **2013**, *51*, 543–547.
25. Kulkarni, N.; Muddapur, U. Biosynthesis of Metal Nanoparticles: A Review. *J. Nanotechnol.* **2014**, *2014*, 1–8. [[CrossRef](#)]
26. Sun, Y. Silver nanowires—unique templates for functional nanostructures. *Nanoscale* **2010**, *2*, 1626–1642. [[CrossRef](#)] [[PubMed](#)]
27. Das, R.; Soni, R.K. Synthesis and surface-enhanced Raman scattering of indium nanotriangles and nanowires. *RSC Adv.* **2017**, *7*, 32255–32263. [[CrossRef](#)]
28. Yousaf, H.; Mehmood, A.; Ahmad, K.S.; Raffi, M. Green synthesis of silver nanoparticles and their applications as an alternative antibacterial and antioxidant agents. *Mater. Sci. Eng. C* **2020**, *112*, 110901. [[CrossRef](#)] [[PubMed](#)]
29. Sawant, V.J.; Sawant, V.J. Biogenic capped selenium nano rods as naked eye and selective hydrogen peroxide spectrometric sensor. *Sens. Bio-Sens. Res.* **2020**, *27*, 100314. [[CrossRef](#)]
30. Ramya, E.; Jyothi, L.; Vardhan, P.V.; Gopal, N.S.R.; Desai, N.R. Optical and biomedical applications of eco-friendly biosynthesized silver nano spheres using zingiber officinale root extract. *Nano Express* **2020**, *1*, 010021. [[CrossRef](#)]
31. Nadagouda, M.N.; Speth, T.F.; Varma, R.S. Microwave-Assisted Green Synthesis of Silver Nanostructures. *Acc. Chem. Res.* **2011**, *44*, 469–478. [[CrossRef](#)]
32. Goh, M.S.; Lee, Y.H.; Pedireddy, S.; Phang, I.Y.; Tjiu, W.W.; Tan, J.M.R.; Ling, X.Y. A Chemical Route to Increase Hot Spots on Silver Nanowires for Surface-Enhanced Raman Spectroscopy Application. *Langmuir* **2012**, *28*, 14441–14449. [[CrossRef](#)] [[PubMed](#)]
33. Wang, Z.; Liu, J.; Chen, X.; Wan, J.; Qian, Y. A Simple Hydrothermal Route to Large-Scale Synthesis of Uniform Silver Nanowires. *Chem. A Eur. J.* **2005**, *11*, 160–163. [[CrossRef](#)] [[PubMed](#)]
34. Luo, L.-B.; Yu, S.-H.; Qian, H.-S.; Gong, J.-Y. Large scale synthesis of uniform silver@carbon rich composite (carbon and cross-linked PVA) sub-microcables by a facile green chemistry carbonization approach. *Chem. Commun.* **2006**, *2006*, 793–795. [[CrossRef](#)]
35. Zhu, J.; Kan, C.; Wu, Y.; Wan, J.; Han, M.; Wang, G. A Novel Discovery of Growth Process for Ag Nanowires and Plausible Mechanism. *J. Nanomater.* **2016**, *2016*, 1–8. [[CrossRef](#)]
36. Sim, H.; Bok, S.; Kim, B.; Kim, M.; Lim, G.-H.; Cho, S.M.; Lim, B. Organic-Stabilizer-Free Polyol Synthesis of Silver Nanowires for Electrode Applications. *Angew. Chem. Int. Ed.* **2016**, *55*, 11814–11818. [[CrossRef](#)] [[PubMed](#)]
37. Yang, C.; Gu, H.; Lin, W.; Yuen, M.M.; Wong, C.P.; Xiong, M.; Gao, B. Silver Nanowires: From Scalable Synthesis to Recyclable Foldable Electronics. *Adv. Mater.* **2011**, *23*, 3052–3056. [[CrossRef](#)]
38. Guo, Z.; Chen, Y.; Wang, Y.-H.; Jiang, H.; Wang, X. Advances and challenges in metallic nanomaterial synthesis and antibacterial applications. *J. Mater. Chem. B* **2020**, *8*, 4764–4777. [[CrossRef](#)] [[PubMed](#)]
39. Sharma, Y.; Kawatra, A.; Sharma, V.; Dhull, D.; Kaushik, S.; Yadav, J.P.; Kaushik, S. In-vitro and in-silico evaluation of the anti-chikungunya potential of *Psidium guajava* leaf extract and their synthesized silver nanoparticles. *VirusDisease* **2021**, *32*, 260–265. [[CrossRef](#)]
40. Sathiyavimal, S.; Vasantharaj, S.; Veeramani, V.; Saravanan, M.; Rajalakshmi, G.; Kaliannan, T.; Al-Misned, F.A.; Pugazhendhi, A. Green chemistry route of biosynthesized copper oxide nanoparticles using *Psidium guajava* leaf extract and their antibacterial activity and effective removal of industrial dyes. *J. Environ. Chem. Eng.* **2021**, *9*, 105033. [[CrossRef](#)]
41. Johan, M.R.; Aznan, N.A.K.; Yee, S.T.; Ho, I.H.; Ooi, S.W.; Singho, N.D.; Aplop, F. Synthesis and Growth Mechanism of Silver Nanowires through Different Mediated Agents (CuCl<sub>2</sub> and NaCl) Polyol Process. *J. Nanomater.* **2014**, *2014*, 1–7. [[CrossRef](#)]
42. Pathak, A.K.; Singh, V.K. SPR Based Optical Fiber Refractive Index Sensor Using Silver Nanowire Assisted CSMFC. *IEEE Photon-Technol. Lett.* **2020**, *32*, 465–468. [[CrossRef](#)]

43. Chung, D.C.K.; Lin, E.S.; Peng, L.; Jiang, X.; Ong, J.W.; Abid, H.A.; Song, Z.; Liew, O.W.; Ng, T.W. Efficient drop reactor processing of methylene blue degradation with silver nanowire catalysts. *Colloids Surf. A Physicochem. Eng. Asp.* **2021**, *610*, 125749. [[CrossRef](#)]
44. Sun, Y. Conversion of Ag Nanowires to AgCl Nanowires Decorated with Au Nanoparticles and Their Photocatalytic Activity. *J. Phys. Chem. C* **2010**, *114*, 2127–2133. [[CrossRef](#)]
45. Pourahmad, A.; Sohrabnezhad, S. Preparation and characterization of Ag nanowires in mesoporous MCM-41 nanoparticles template by chemical reduction method. *J. Alloys Compd.* **2009**, *484*, 314–316. [[CrossRef](#)]
46. Kimura, H.; Okada, G.; Kato, T.; Nakauchi, D.; Kawaguchi, N.; Yanagida, T. Radio-photoluminescence properties of silver-doped cesium chloride transparent ceramics. *J. Lumin.* **2021**, *236*, 118099. [[CrossRef](#)]
47. Parente, M.; Van Helvert, M.; Hamans, R.F.; Verbroekken, R.; Sinha, R.; Bieberle-Hütter, A.; Baldi, A. Simple and Fast High-Yield Synthesis of Silver Nanowires. *Nano Lett.* **2020**, *20*, 5759–5764. [[CrossRef](#)] [[PubMed](#)]
48. Radhakrishnan, S. Synthesis and Characterization of Silver Nanoparticles from Psidium Guajava Leaf Extract. *Int. J. Pharm. Sci. Nanotechnol.* **2021**, *14*, 5634–5638. [[CrossRef](#)]
49. Le, N.T.T.; Trinh, B.T.D.; Nguyen, D.H.; Tran, L.D.; Luu, C.H.; Thi, T.T.H. The Physicochemical and Antifungal Properties of Eco-friendly Silver Nanoparticles Synthesized by Psidium guajava Leaf Extract in the Comparison with Tamarindus indica. *J. Clust. Sci.* **2021**, *32*, 601–611. [[CrossRef](#)]
50. Sandhiya, V.; Gomathy, B.; Sivasankaran, M.R.; Thirunavukkarasu, P.; Mugip Rahaman, A.; Asha, S. Green synthesis of silver nanoparticles from Guava (Psidium guajava Linn.) leaf for antibacterial, antioxidant and cytotoxic activity on HT-29 cells (Colon cancer). *Ann. Rom. Soc. Cell Biol.* **2021**, *25*, 20148–20163.
51. Nguyen, T.D.; Nguyen, D.P.; Hoang, Y.H.; Nguyen, T.T.; Nguyen, H.T. Rapid synthesis of silver nanoparticles using the extract of Psidium guajava leaf based on light-emitting diodes irradiation. *Chem. Pap.* **2021**, *75*, 5623–5631. [[CrossRef](#)]
52. Zayed, M.; Ghazal, H.; Othman, H.; Hassabo, A.G. Psidium Guajava leave extract for improving ultraviolet protection and antibacterial properties of cellulosic fabrics. *Biointerf. Res. Appl. Chem.* **2021**, *12*, 2022.
53. Ghosh, T.; Chattopadhyay, A.; Mandal, A.C.; Pramanik, S.; Mukherjee, S.; Kuiri, P.K. Spectroscopic, microscopic and antibacterial studies of green synthesized Ag nanoparticles at room temperature using Psidium guajava leaf extract. *Korean J. Chem. Eng.* **2021**, *1–11*. [[CrossRef](#)]
54. Han, W.; Dong, F.; Han, W.; Tang, Z. A strategy to construct uniform MOFs/PAN nanowire derived bead-like Co<sub>3</sub>O<sub>4</sub> for VOC catalytic combustion. *Chem. Commun.* **2020**, *56*, 14307–14310. [[CrossRef](#)] [[PubMed](#)]
55. Hayashi, Y.; Fujita, K.; Narira, I.; Inoue, M.; Takizawa, H. Synthesis and optimization of silver nanowire transparent conductive film by organic needle-shaped precursor painting reduction method. In Proceedings of the 2016 IEEE 16th International Conference on Nanotechnology (IEEE-NANO), Sendai, Japan, 22–25 August 2016; pp. 257–260.
56. Satsangi, N. Synthesis and Characterization of Biocompatible Silver Nanoparticles for Anticancer Application. *J. Inorg. Organomet. Polym. Mater.* **2019**, *30*, 1907–1914. [[CrossRef](#)]
57. Nagasundari, S.M.; Muthu, K.; Kaviyarasu, K.; Al Farraj, D.A.; Alkufeidy, R.M. Current trends of Silver doped Zinc oxide nanowires photocatalytic degradation for energy and environmental application. *Surf. Interfaces* **2021**, *23*, 100931. [[CrossRef](#)]
58. Tang, Y.; He, W.; Wang, S.; Tao, Z.; Cheng, L. One step synthesis of silver nanowires used in preparation of conductive silver paste. *J. Mater. Sci. Mater. Electron.* **2014**, *25*, 2929–2933. [[CrossRef](#)]
59. Sciacca, B.; Yalcin, A.O.; Garnett, E. Transformation of Ag Nanowires into Semiconducting AgFeS<sub>2</sub> Nanowires. *J. Am. Chem. Soc.* **2015**, *137*, 4340–4343. [[CrossRef](#)]
60. Liu, X.; Luo, A.J.; Zhu, J. Size Effect on the Crystal Structure of Silver Nanowires. *Nano Lett.* **2006**, *6*, 408–412. [[CrossRef](#)]
61. Carolin, C.F.; Kumar, P.S.; Joshiba, G.J. Sustainable approach to decolourize methyl orange dye from aqueous solution using novel bacterial strain and its metabolites characterization. *Clean Technol. Environ. Policy* **2021**, *23*, 173–181. [[CrossRef](#)]
62. Wu, T.; Kou, Y.; Zheng, H.; Lu, J.; Kadasala, N.R.; Yang, S.; Guo, C.; Liu, Y.; Gao, M. A Novel Au@Cu<sub>2</sub>O-Ag Ternary Nanocomposite with Highly Efficient Catalytic Performance: Towards Rapid Reduction of Methyl Orange under Dark Condition. *Nanomaterials* **2019**, *10*, 48. [[CrossRef](#)]
63. Shan, R.; Lu, L.; Gu, J.; Zhang, Y.; Yuan, H.; Chen, Y.; Luo, B. Photocatalytic degradation of methyl orange by Ag/TiO<sub>2</sub>/biochar composite catalysts in aqueous solutions. *Mater. Sci. Semicond. Process.* **2020**, *114*, 105088. [[CrossRef](#)]
64. Rodwihok, C.; Wongratanaphisan, D.; Van Tam, T.; Choi, W.M.; Hur, S.H.; Chung, J.S. Cerium-Oxide-Nanoparticle-Decorated Zinc Oxide with Enhanced Photocatalytic Degradation of Methyl Orange. *Appl. Sci.* **2020**, *10*, 1697. [[CrossRef](#)]
65. Ramos, P.G.; Luyo, C.; Sánchez, L.A.; Gomez, E.D.; Rodriguez, J.M. The Spinning Voltage Influence on the Growth of ZnO-rGO Nanorods for Photocatalytic Degradation of Methyl Orange Dye. *Catalysts* **2020**, *10*, 660. [[CrossRef](#)]
66. Raj, S.; Singh, H.; Trivedi, R.; Soni, V. Biogenic synthesis of AgNPs employing Terminalia arjuna leaf extract and its efficacy towards catalytic degradation of organic dyes. *Sci. Rep.* **2020**, *10*, 1–10. [[CrossRef](#)]
67. Kumari, P.; Meena, A. Green synthesis of gold nanoparticles from Lawsoniainermis and its catalytic activities following the Langmuir-Hinshelwood mechanism. *Colloids Surf. A Physicochem. Eng. Asp.* **2020**, *606*, 125447. [[CrossRef](#)]
68. Hussain, I.; Farooqi, Z.H.; Ali, F.; Begum, R.; Irfan, A.; Wu, W.; Wang, X.; Shahid, M.; Nisar, J. Poly(styrene@N-isopropylmethacrylamide-co-methacrylic acid)@Ag hybrid particles with excellent catalytic potential. *J. Mol. Liq.* **2021**, *335*, 116106. [[CrossRef](#)]